Development of a sparse aperture test-bed utilizing pupil-plane imaging.

Douglas Jameson
AFRL Sensors Directorate
David Rabb
AFRL Sensors Directorate
Capt. James Roche
AFRL Sensors Directorate

1. Abstract

Sparse aperture imaging provides the opportunity to achieve high resolutions image with groups of smaller apertures rather than a large single aperture. Eliminating large monolithic apertures provides both a cost and weight reduction among other possible benefits. Imaging with sparse apertures requires that both amplitude and phase of the incident field be captured so that an effectively larger aperture can be synthesized. Amplitude is easily captured using traditional imaging systems however capturing phase requires more advanced methods such as interferometry or phase retrieval algorithms. The design of sparse aperture imaging arrays has previously been discussed theoretically and through computer simulations however experimental verification is still needed. A sparse test bed is proposed and initial designs are discussed. The test bed provides the ability to experiment with various sparse aperture array patterns as well as sub-aperture spacing, allowing comparison of results with theory. The first step in construction of the test beds is the design of individual telescopes which will allow the field to be recorded at each of the sub-apertures by utilizing digital holography, a method referred to as pupil plane imaging. Pupil plane imaging using spatial heterodyning is described and the theory is laid out, which will allow for the recovery of the target field from a recorded interference pattern. It is demonstrated how a pupil plane imaging telescope can be used to perform lens-less imaging, effectively forming the image digitally. Expressions, which simplify focusing the resulting image on the target, are derived and experimental results are provided. Compact telescopes are developed which will provide the foundation of a sparse aperture test bed and image results are given for a prototype telescope.

2. Introduction

One of the main driving forces behind sparse aperture imaging is a general reduction in equipment size and weight needed to create high resolution images. Traditional imaging systems tend to increase in volume with the cube of the aperture diameter. As a result the imaging system can quickly increase not only in size but also in weight. Sparse aperture imaging provides the ability to create high resolution images by sampling the backscattered wave-front across multiple sub-apertures, and then synthesizing the resulting images into a single higher resolution image. Due to the fact that the individual sub-apertures each utilize smaller aperture diameters than the effective diameter of the high resolution image there is a net savings in system volume and therefore weight for an analogous resolution.

The first logical step in designing a sparse aperture system would be to predict the resolving power based on the sparse aperture array geometry. Desirable patterns have been identified by Miller et, al. [1] for static systems. These patterns are known as Golay arrays and feature non-redundant geometries [2] which allows for efficient imaging. Patterns such as the Golay arrays provide background for modeling point spread functions as well as modulation transfer functions.

In an effort to understand the phenomenology, sensitivity, and design parameters required by these systems the total system can be broken up into several sub-areas such as: array selection, field recovery, synthesis algorithms, etc. Regarding field recovery each sub-aperture must be able to capture the field information so that the high resolution image can be synthesized. Holography and specifically digital holography provide a technique for capturing the required fields [3]. A capable method which has recently been described by Marron et. al. [4] utilizes digital holography to capture the field information. This method is known as spatial-heterodyned pupil-plane imaging and is the focus of the current work.

3. Theory

In order to synthesize a high-resolution image field data is captured at each of the sub-apertures using a process known as pupil-plane imaging. This process is analogous to digital holography while a specific technique known as spatial heterodyning is used in the current research. The digital holography technique is illustrated in Fig. 1.
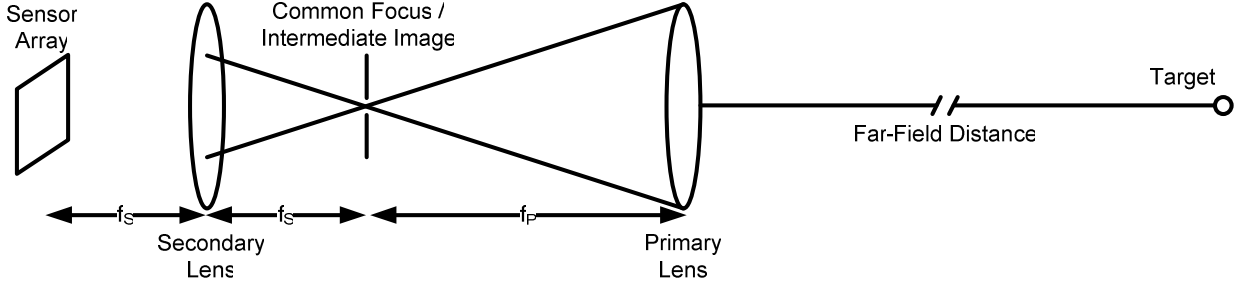

Fig. 1. The target is located in the far-field of the primary lens. The resulting wavefront is relayed (with magnification) to the sensor. The local oscillator is not shown.

In this process a target defined by the function $t(x_0,y_0)$ is located in the far-field of the imaging system. The paraxial field at the primary lens of the telescope is given by the Fraunhoffer diffraction pattern of the target as defined by [5]

$$T_1(x_1, y_1) = \frac{e^{jkz} e^{j\frac{k}{2z}\left(x_1^2 + y_1^2\right)}}{j\lambda z} \int_{-\infty}^{\infty}\int_{-\infty}^{\infty} t(x_0, y_0)\exp\left[-j\frac{2\pi}{\lambda z}(x_1 x_0 + y_1 y_0)\right]dx_0 dy_0, \tag{1}$$

where z is the propagation distance, $x_1 y_1$ is the coordinate plane at the front of the primary lens, and λ is the wavelength of the light. This is a Fourier transform of the initial field $t(x_0,y_0)$ with the associated phase terms. We can now express Equation 1 as

$$T_1(x_1, y_1) = \frac{e^{jkz} e^{j\frac{k}{2z}\left(x_1^2 + y_1^2\right)}}{j\lambda z} \Im\{t(x_0, y_0)\}. \tag{2}$$

The first lens creates an intermediate image at the common focus in the telescope. The expression for the associated field formed by a thin lens is given by [5]

$$T_2(x_2, y_2) = \frac{e^{j\frac{k}{2f_P}\left(x_2^2 + y_2^2\right)}}{j\lambda f_P} \Im\{P(x_1, y_1)T_1(x_1, y_1)\}, \tag{3}$$

where $x_2 y_2$ is the coordinate system at the intermediate image, and f_P is the focal length of the primary and $P(x_1,y_1)$ is the pupil function defined by the aperture size of the primary lens. Lastly the intermediate image plane is located at the front focal plane of the secondary lens and the field at the back focal plane of this lens is given by [5]

$$T_3(x_3, y_3) = \Im\{T_2(x_2, y_2)\}, \tag{4}$$

where the quadratic phase factors can be dropped due to the input field being located at the front focal plane of the thin lens. Furthermore the constant terms will be dropped for convenience. Equations 2 through 4 are combined to find the resulting field on the sensor array yielding

$$T_3(x_3, y_3) = \Im \left\{ \frac{e^{j\frac{k}{2f_P}(x_2^2+y_2^2)}}{j\lambda f_P} \Im \left[P(x_1, y_1) \frac{e^{jkz} e^{j\frac{k}{2z}(x_1^2+y_1^2)}}{j\lambda z} \Im\{t(x_0, y_0)\} \right] \right\}. \tag{5}$$

This expression is simplified by using the convolution theorem repeatedly which yields

$$T_3(x_3, y_3) = \Im \left(\frac{e^{j\frac{k}{2f_P}(x_2^2+y_2^2)}}{j\lambda f_P} \right) \otimes P(-x_1, -y_1) \frac{e^{jkz} e^{j\frac{k}{2z}(x_1^2+y_1^2)}}{j\lambda z} \Im\{t(-x_0, -y_0)\}, \tag{6}$$

here the symmetry of the circular pupil is used to express $P(-x,-y)$ as $P(x,y)$ and it is assumed that $(x_1^2+y_1^2) \ll z$ which is a likely scenario due to the fact we are operating in the far field. The resulting expression for the field incident on the sensor is then given by

$$T_3(x_3, y_3) = \frac{e^{jkz}}{j\lambda z} \Im \left\{ \frac{e^{j\frac{k}{2f_P}(x_2^2+y_2^2)}}{j\lambda f_P} \right\} \otimes P(x_1, y_1) \Im\{t(-x_0, -y_0)\}. \tag{7}$$

Finally, the local oscillator (LO) is injected, through a folded path, as a point in the intermediate image at the common focus within the telescope. The LO is injected as an off-axis point source in the intermediate image plane y way of a beam splitter. The LO is propagated through the secondary lens and results in a tilted plane wave as given by

$$L(x_3, y_3) = A \exp(-jk(\sin\theta_x x_3 + \sin\theta_y y_3)), \tag{8}$$

where the plane wave is assumed to have uniform amplitude given by A and the tilt is given at angles of θ_x and θ_y. This process, known as spatial heterodyne, has multiple benefits including the ability to reconstruct the target image outside of the DC fringe noise. The two fields incident on the sensor array are detected as a fringe pattern with bias fringes determined by the tilt of the LO as with a Leith-Upatnieks hologram. The detected intensity is expressed as

$$I(x_3, y_3) = |T_3(x_3, y_3) + L(x_3, y_3)|^2 = |T_3|^2 + |L|^2 + T_3^* L + T_3 L^*. \tag{9}$$

The fringe pattern is captured with a sensor array (CMOS, CCD, or FPA), digitized and stored as an image. The digital hologram can be reconstructed by applying a Fourier transform to the captured fringe pattern. Applying a transform to the fringe pattern yields

$$\begin{aligned} R(x_4, y_4) &= \Im\left\{ |T_3|^2 + |L|^2 + T_3^* L + T_3 L^* \right\} \\ &= \Im\{|T_3|^2\} + \Im\{|L|^2\} + \Im\{T_3^*\} \otimes \Im\{L\} + \Im\{T_3\} \otimes \Im\{L^*\} \end{aligned} \tag{10}$$

The first two terms represent the autocorrelation of the incident target and local oscillator fields while the last two terms represent convolutions between the target field and the LO in the form of an off-axis point source. The image recovery is shown by substituting Equation 7 and Equation 8 into the fourth term of Equation 10 such that

$$\Im\{T_3\}\otimes\Im\{L^*\}=\Im\left\{\frac{e^{jkz}}{j\lambda z}\Im\left\{\frac{e^{j\frac{k}{2f_P}\left(x_2^2+y_2^2\right)}}{j\lambda f_P}\right\}\otimes P(x_1,y_1)\Im\{t(-x_0,-y_0)\}\right\}$$

$$\otimes\Im\{A\exp\left(jk\left(\sin\theta_x x_3+\sin\theta_y y_3\right)\right)\}. \tag{11}$$

Applying the convolution theorem yields

$$\Im\{T_3\}\otimes\Im\{L^*\}=\frac{e^{jkz}}{j\lambda z}\frac{e^{j\frac{k}{2f_P}\left(x_2^2+y_2^2\right)}}{j\lambda f_P}\left(\Im\{P(x_1,y_1)\}\otimes t(x_0,y_0)\right)\otimes A\delta(x_3-X,y_3-Y). \tag{12}$$

where $X=f_{LO}\sin\theta_x$ and $Y=f_{LO}\sin\theta_y$. Therefore the target field (blurred by the primary lens aperture and having accumulated some quadratic curvature) has been captured and has been translated in the resulting target plane. Similarly the third term represents the phase conjugate image and can be expressed as

$$\Im\{T_3^*\}\otimes\Im\{L\}=\frac{e^{-jkz}}{-j\lambda z}\frac{e^{-j\frac{k}{2f_P}\left(x_2^2+y_2^2\right)}}{-j\lambda f_P}\left(\Im\{P(x_1,y_1)\}\otimes t^*(-x_0,-y_0)\right)\otimes A\delta(x_3+X,y_3+Y). \tag{13}$$

An illustration of the resulting reconstruction plane is shown in Fig. 2.
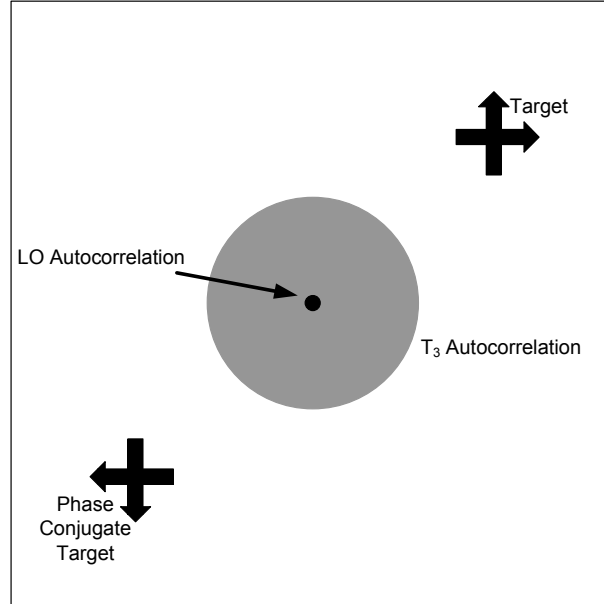

Fig. 2. An illustration of the reconstructed image plane showing the autocorrelation terms, the reconstructed target and the reconstructed phase-conjugate target.

4. Experiment

The pupil-plane imaging system is designed with regard to the sensor array's ability to Nyquist sample the interference fringe pattern. Specifically the pixel-pitch of the sensor determines the spatial sampling period and thus the period of the shortest recordable fringe. The camera used here is a Lumenera LU120M monochromatic camera with a pixel pitch of 6.7 μm. As mentioned above the spatial heterodyne LO is effectively a tilted plane wave and the ideal tilt angle can be found given the pixel pitch of this sensor. As shown in Fig. 2 above the ideal center location for the target image would be centered in one of the quadrants. Given that the image plane illustrated in

Fig. 2 is actually the Fourier plane of the captured fringe pattern the edges of the image plane correspond to the Nyquist sampling rate of 2 pixels per fringe. A point target located at the center of the quadrant would therefore have a sampling rate of 4 pixels per fringe in both the horizontal and vertical directions. For an object located down the optic axis of the telescope system a LO tilt angle can be found using $\theta\Lambda \approx \lambda$ which for a wavelength of 632.9 nm and a fringe period of 26.8 µm yields a tilt angle of approximately 1.35°. Taking this result along with the illustration given in Fig. 2 yields a full angle field of view of 2.7° so that the target space will fit un-aliased within a single quadrant of the reconstructed image. The telescope magnification is chosen so that the telescope will balance overall length and ease of construction with the efficiency of capturing photons. In other words, the circular pupil-plane imaged at the detector will either under fill or overfill the CCD either wasting pixels or photons, respectively. The trade-space between pixel and photon efficiencies for our detector and a 2 inch optic is shown in Fig. 3 below. In the current design a magnification of 6x was chosen due to the availability of optics.
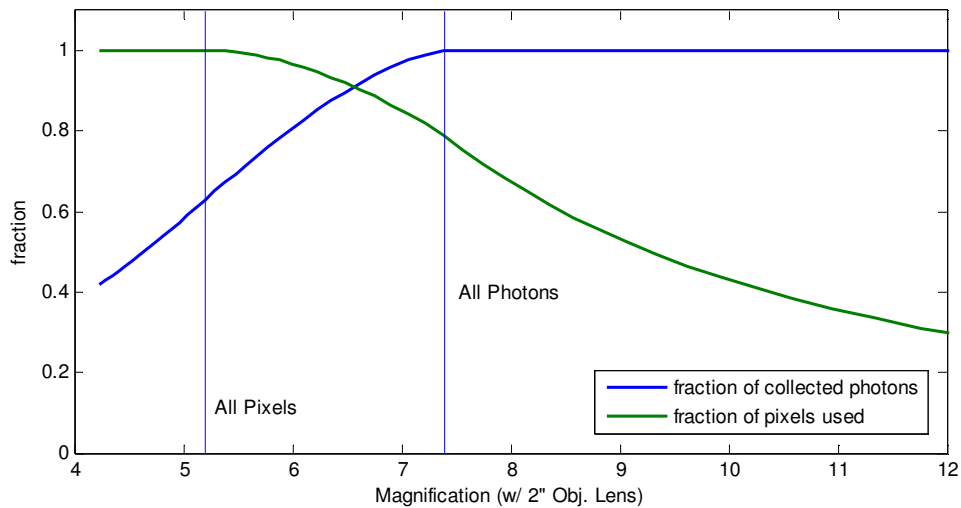

Fig. 3. Pixel and photon efficiency vs. telescope magnification.

The final imaging system design is shown in Fig. 4 below. The telescope has been stopped at the intermediate image plane which yields a target-space full angle FOV of 0.45° or 7.9 *mrad*.
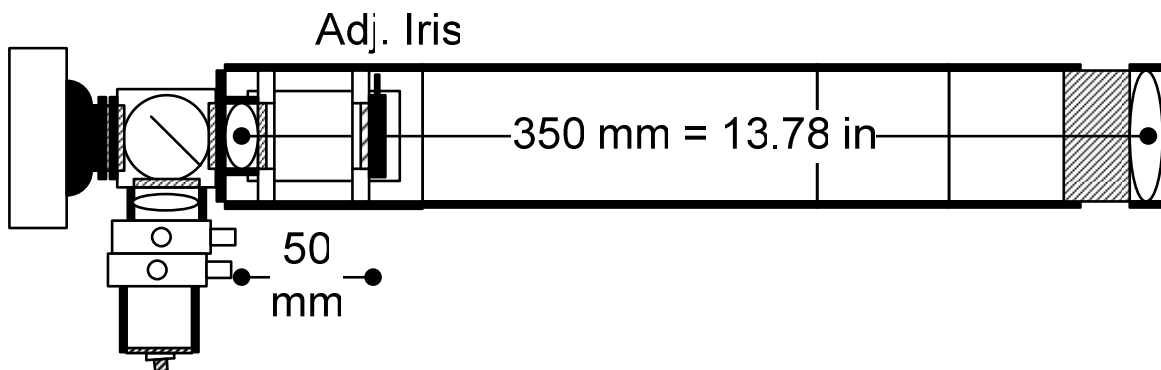

Fig. 4. Telescope design with LO injection providing a tilt angle of approximately 1.35°.

An ISO12233 resolution chart is used as the target which is placed in front of an eight inch off-axis paraboloid mirror with a focal length of 24 inches. The mirror collimates the light across a large footprint thus projecting the target to the far-field and the small size of the resolution chart allows for aberrations to be kept at a minimum.

A second experiment involves synthesis of three apertures arrayed in a horizontal pattern as in Fig. 5. In this case a point target is created through the use of a single mode fiber. The target is imaged by three horizontally

arrayed telescopes and phase correction is applied through use of Zernike polynomials for each of the recovered phase fronts. Due to the nature of the target we expect flat phase at each of the recovered pupils and the application of Zernike polynomials flattens the phase and mitigating the static system aberrations for the on-axis point sources thus allowing imaging at the diffraction limit. The pupils are then registered and a Fourier transform provides the final synthesized image. It is expected that resolution will be increased in the horizontal direction with respect to the vertical direction. This resolution increase will be evident by a narrowing of the amplitude impulse response in the horizontal direction.
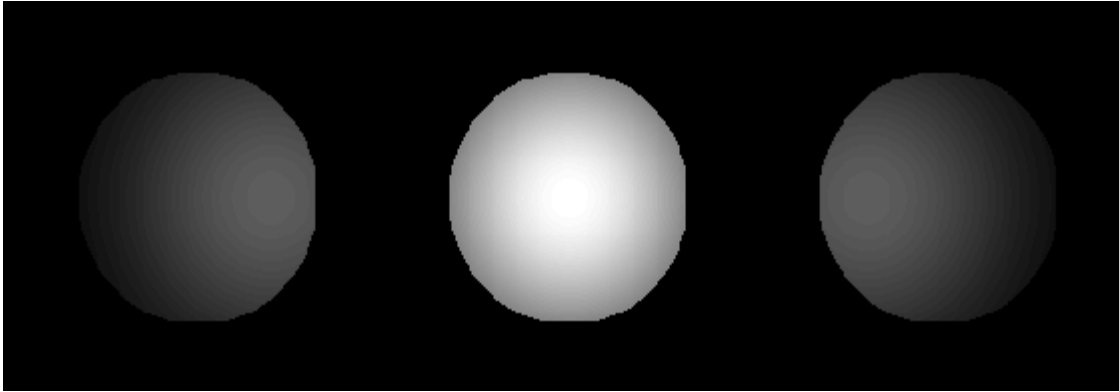

Fig. 5. The three horizontally arrayed apertures are shown including the approximate illumination encountered in the experiment.

5. Results

A single telescope system is used to image the target according to the theory laid out above. A captured fringe pattern is shown in Fig. 6.
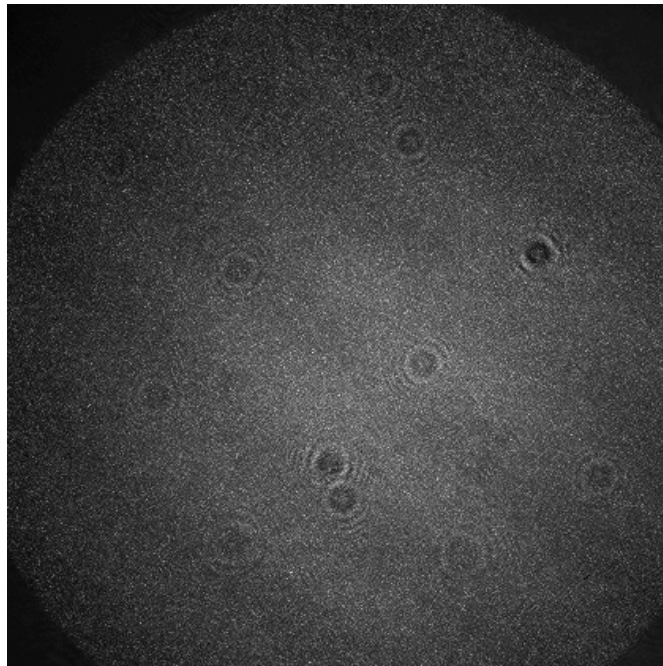

Fig. 6. Captured fringe pattern after interference of pupil field with tilted LO.

The fringe image suffers from some noise from dust particles on the lenses which will likely affect image quality. The choice of magnification of 6x yields an under-filled CCD array, thus the corners appear dark. It should be noted that due to the camera's form-factor it is impossible to align the sensor at the back focal plane of the secondary lens.

As a result there is some quadratic curvature added to the field due to defocus. The Fourier transform is applied to the fringes which forms the reconstructed image(s) as shown in Fig. 7 and Fig. 8.
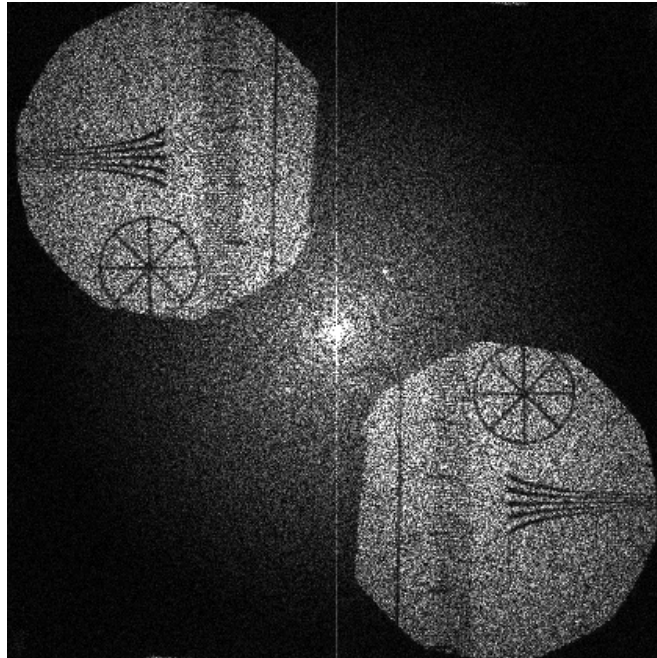

Fig. 7.   The reconstructed images are shown along with the expected autocorrelation terms. The autocorrelation terms were allowed to saturate the bitmap in order to bring out the target. All four features are visible including the image and the phase-conjugate image as well as the LO autocorrelation (white spot at the center) and the target field autocorrelation (the gray cloud in the background).
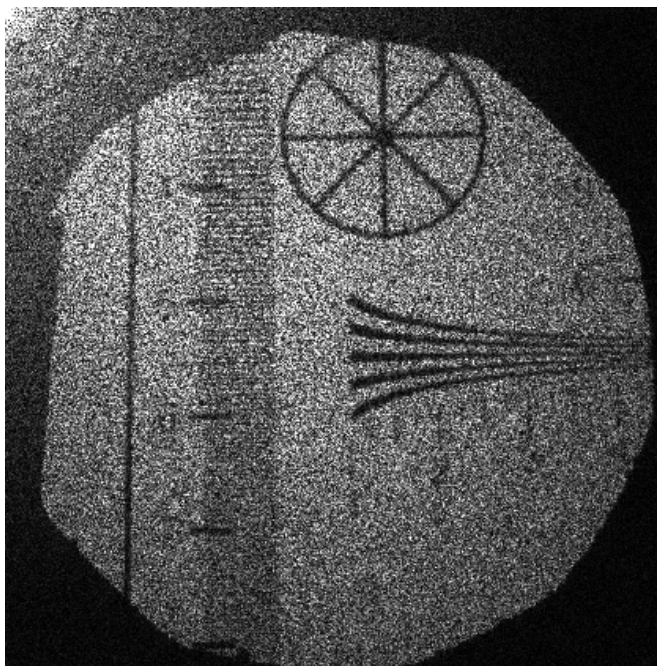

Fig. 8. A zoomed-in version of the reconstructed image.

The results of the horizontal aperture array synthesis experiment are shown in Fig. 9 along with the theoretical prediction. Diffraction limited results were achieved by flattening the phase through the use of Zernike polynomials. Viewing the cross sections in Fig. 9 shows that the horizontal impulse response indeed has a narrower central peak along the horizontal dimension. These results are encouraging and illustrate the ability of pupil plane imaging systems to overcome static aberrations.
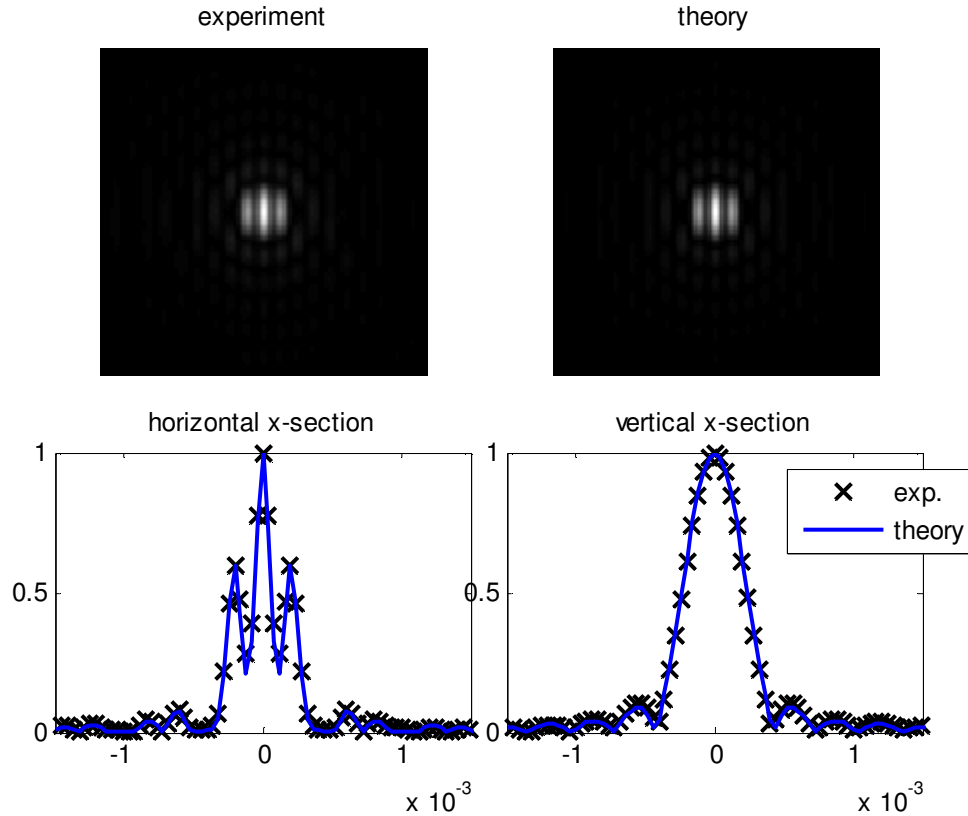

Fig. 9. Normalized impulse response from three horizontally arrayed experimental apertures along with the theoretical results.

6. Conclusion

In order to drive imaging systems towards smaller volumes and lower weights it is necessary to invent novel methods for achieving small diffraction limited spot sizes. Sparse aperture imaging provides a possible solution to this dilemma. However, in order to synthesize a higher resolution image the field data must be captured at each of the sub-apertures in the array. Pupil-plane imaging offers an interesting solution towards capturing the field information at each of the sub-apertures.

Currently multiple imaging systems have been constructed and they are capable of imaging the target simultaneously. Synthesizing an image of a single point target is easily accomplished down to the diffraction limit by flattening the recorded phases and registering the pupil locations. This test-bed hardware will allow tolerance experiments, link-budget verification, and algorithm test data to be collected. Work is now focused on developing algorithms to synthesize the individual sub-aperture images into a higher resolution image for more complex targets.

7. Acknowledgements

References

1. Nicholas J. Miller, Matthew P. Dierking, and Bradley D. Duncan, Optical Sparse Aperture Imaging, *Applied Optics*, Vol. 45, Issue 23, pp 5933-5943 (2007).

2. M. Golay, Point Arrays Having Compact Non-redundant Autocorrelations, *Journal of the Optical Society of America*, Vol. 61, pp 272-273 (1971).

3. Joseph C. Marron and Richard L. Kendrick, Distributed Aperture Active Imaging, Proc. SPIE, Vol. 6550 (2007).

4. Powell, Rodney M., Digital Holography, AFRL-MN-EG-RT-2000-7045, Feb. 2000.

5. Joseph W. Goodman, *Introduction to Fourier Optics, Second Edition*. McGraw-Hill. Boston, 1996.